Journal of Photonics for Energy

PhotonicsforEnergy.SPIEDigitalLibrary.org

Bioinspired molecular electrets: bottom-up approach to energy materials and applications

Jillian M. Larsen
Eli M. Espinoza
Valentine I. Vullev

SPIE.

Bioinspired molecular electrets: bottom-up approach to energy materials and applications

Jillian M. Larsen,[a] Eli M. Espinoza,[b] and Valentine I. Vullev[a,b,c,d,*]

[a]University of California, Riverside, Department of Bioengineering, 217 MSE Building, Riverside, California 92521, United States

[b]University of California, Riverside, Department of Chemistry, 501 Big Springs Road, Riverside, California 92521, United States

[c]University of California, Riverside, Department of Biochemistry, 1463 Boyce Hall, Riverside, California 92521, United States

[d]University of California, Riverside, Materials Science and Engineering Program, 307 MSE Building, Riverside, California 92521, United States

Abstract. The diversity of life on Earth is made possible through an immense variety of proteins that stems from less than a couple of dozen native amino acids. Is it possible to achieve similar engineering freedom and precision to design electronic materials? What if a handful of non-native residues with a wide range of characteristics could be rationally placed in sequences to form organic macromolecules with specifically targeted properties and functionalities? Referred to as molecular electrets, dipolar oligomers and polymers composed of non-native aromatic beta-amino acids, anthranilamides (Aa) provide venues for pursuing such possibilities. The electret molecular dipoles play a crucial role in rectifying charge transfer, e.g., enhancing charge separation and suppressing undesired charge recombination, which is essential for photovoltaics, photocatalysis, and other solar-energy applications. A set of a few Aa residues can serve as building blocks for molecular electrets with widely diverse electronic properties, presenting venues for bottom-up designs. We demonstrate how three substituents and structural permutations within an Aa residue widely alter its reduction potential. Paradigms of diversity in electronic properties, originating from a few changes within a basic molecular structure, illustrate the promising potentials of biological inspiration for energy science and engineering. © *2015 Society of Photo-Optical Instrumentation Engineers (SPIE)* [DOI: 10.1117/1.JPE.5.055598]

Keywords: dipole; photoinduced; charge transfer; ionization energy; solar; anthranilic.

Paper 15024SS received Mar. 7, 2015; accepted for publication Apr. 16, 2015; published online May 15, 2015.

1 Introduction

This article describes the design rationale for oligomers and polymers with large permanent electric dipoles, i.e., molecular electrets, composed of anthranilamide (Aa) residues (Fig. 1).[1–3] A comparison with biopolymers illustrates the basis for referring to the Aa molecular electrets as bioinspired. For improved charge-transfer (CT) properties, the Aa electrets incorporate features from different biomolecular structures to form non-native systems beneficial for electronic and photonic materials for energy applications.

Understanding and controlling CT at a nanometer scale is paramount for solar-energy harvesting, conversion, and storage.[4–8] Local electric fields, originating from molecular dipoles, can strongly affect the behavior of charge carriers. Molecular-scale engineering of field profiles along CT pathways provides an incomparable means for controlling the direction and the efficiency of electron and hole transduction. Therefore, molecular electrets can play a central role in the bottom-up designs of hybrid electronic materials and energy-conversion devices.

Oligomers and polymers of aromatic β-amino acids, i.e., Aa residues, have two uniquely combined features: (1) ordered amide and hydrogen bonds resulting in electric dipoles of

*Address all correspondence to: Valentine I. Vullev, E-mail: vullev@ucr.edu

Fig. 1 Bioinspired molecular electrets composed of anthranilamide (Aa) residues: (a) a segment of a molecular electret—$Aa^{(i)} - Aa^{(j)} - Aa^{(k)} - Aa^{(l)} - Aa^{(m)} - Aa^{(n)}$; (b) origin of the Aa dipole from ordered orientation of amide bonds and from the polarization upon hydrogen bonding.

about 3 D/residue, oriented from the N- to the C-termini (Fig. 1)[9] and (2) extended π-conjugation along the macromolecular backbone that can prove essential for mediating long-range CT.[10] Our computational and experimental studies demonstrated that Aa conjugates possess permanent electric dipoles, i.e., they are indeed molecular electrets.[2,9] Comparing the extent of deshielding (i.e., relative acidity) of the amide protons as determined from nuclear magnetic resonance (NMR) studies provided experimental confirmation that the total molecular dipoles are oriented form the N- to the C-termini of the Aa conjugates.[2]

We have demonstrated that an Aa residue can act as a molecular rectifier (or a diode), showing preference of electron transfer (ET) toward the C-terminus.[1] This emphasis on rectification of CT, rather than charge transport, allows for assessing the effects induced by small organic residues or short oligomers without the interference from the contacts with conducting and semiconducting substrates.[11,12] Interfacial charge transport and CT "hold" the key for improving energy-conversion efficiencies of materials and devices.[4,13,14] Molecular-level understanding of charge-transfer rectification, implemented with a rational control of surfaces and interfaces,[5,15–17] provides the venues for such efficiency improvements.

The magnitude of CT rectification for a single Aa residue is comparable with the rectification exerted by peptide helices comprising more than 10 amino acid residues.[1] The molecular dipoles have a dominating contribution toward this rectification effect. The asymmetry in electron-density distribution, induced by the positions of the substituents, and the molecular dynamics also contribute to the CT processes. The latter affects the photoinduced charge separation kinetics, while the former affects the consequent charge recombination.[1]

To truly benefit from the promising CT properties of Aa, it is essential to achieve structural diversity of these electret conjugates, leading to wide variety of electronic functionalities. Extending principles from proteomics to the design of widely diverse molecular electrets places a demand on developing sets of their building blocks, i.e., the non-native Aa residues, with different electronic properties.

Herein, we describe the rationale behind bringing structural features from different classes of biomacromolecules (i.e., proteins and nucleic acids) to design Aa molecular electrets in the search of improved CT properties that are not inherent for living systems. We focus on a set of Aa residues that are chemically modified with electron-donating substituents (at R_1 and R_2, Fig. 1) for lowering the ionization energies and improving hole-transfer capabilities. Replacing the hydrogen at R_2 with three types of substituents with different electron-donating propensity causes negative shifts in the Aa reduction potential, amounting to about 0.1, 0.3, and 1 V. Moving an electron-donating group (EDG) from R_2 to R_1 results in a positive shift in the reduction potentials of about 0.1 to 0.3 V, which is indicative of an increase in the ionization energy. Discussion of their rectification and other CT properties illustrates the potential impact that the diversity in Aa molecular electrets can have on electronic materials and energy conversion.

2 CT Molecular Electrets: Practical Ideas from Structural Biology

Electrets are dielectrics with permanent electric polarization. The polarization can originate from volume-embedded or surface-trapped charges (i.e., real-charge electrets), or from codirectionally ordered electric dipoles (i.e., dipole-polarization or dipolar electrets).[18,19] The lack of directionality of electrostatic interactions and ionic bonds governs the dynamics and the complexity in the

behavior of real-charge electrets that encompass "space-charge" and "surface-charge electrets."[20,21] Conversely, the defined directionality of covalent bonds (which, indeed, are also electric in nature) provides a key advantage for arranging noncharged molecular dipolar moieties. For molecular dipoles, patterns of covalent bonding keep the displacement of the centers of positive and negative charges more or less permanently fixed. Therefore, dipolar electrets, which are electrostatic analogues of magnets,[22] provide an important venue for the design and development of macromolecules and materials for electronic and energy applications.

Biology presents some of the best examples of molecular electrets and the utility of their electronic properties. Peptide bonds are aliphatic amides (with permanent dipoles of about 4 D)[23] that hold together the protein backbones. In protein α-helices, the peptide bonds are codirectionally oriented along the helix axes (Fig. 2), resulting in substantial electrical polarization of these macromolecular secondary conformers,[24–26] i.e., protein α-helices are biomolecular electrets.

A network of hydrogen bonds, which are also aligned along the helix axes supporting these protein structures (Fig. 2), further enhances the total macromolecular dipoles of protein α-helices. The hydrogen bonding between the carbonyl oxygens and amide hydrogens from peptide bonds on neighboring helix turns causes a collective shift in electron density from the oxygens to the hydrogens, i.e., it causes polarization that is in the direction of the amide dipoles. This effect, however, does not result in negatively charged hydrogens and positively charged oxygens. Rather, the oxygens in the peptide bonds are negatively polarized and upon hydrogen bonding, some of this partial negative charge shifts toward the N–H bond of an amide on the neighboring turn. The ordered hydrogen and peptide bonds in the α-helices result in their intrinsic electric dipoles of about 5 D/residue, pointing from the C- to the N-termini (Fig. 2).[27]

Other protein helices also exhibit dipole-induced polarization. Similar to α-helices, alignment of hydrogen and amide bonds in 3_{10}-helices results in intrinsic electric dipoles (4.5 D/residue) pointing from the C- to the N-termini.[27] In fact, 3_{10}-helices are tight-wound analogues of α-helices: i.e., 3_{10}-helices contain three residues per turn and each hydrogen bond closes a backbone loop comprising 10 atoms. Indeed, protein α-helices are 3.6_{13} helices.

Polyproline helices exhibit another interesting set of electronic properties. Proline is a native amino acid with a rigid structure and a secondary α-amine. Therefore, polyprolines assume helical conformations without hydrogen bonding, making their intrinsic dipoles smaller than the dipoles of α-helices.[27] In the two types of polyproline helices, type I and type II, the peptide bonds have different conformations and their dipoles are orientated differently. Type I comprises "cis" amides inducing a ground-state dipole of 4.1 D/residue (pointing from the N- to the C-terminus), and type II with "trans" amides has a dipole of 1.5 D/residue (pointing from the C- to the N-terminus). Therefore, conformational changes back and forth from type I to type II polyproline helices switch the direction of their polarization,[27] which is a unique feature of these biomolecular electrets.

The dipole-generated electric fields in the proximity of protein helices amounts to about 10^8 to 10^9 V/m, which proves important for ET and ion-transport processes in living organisms.[28–31] In synthetic polypeptide helices, the intrinsic dipoles rectify the directionality of CT.[32–37] The

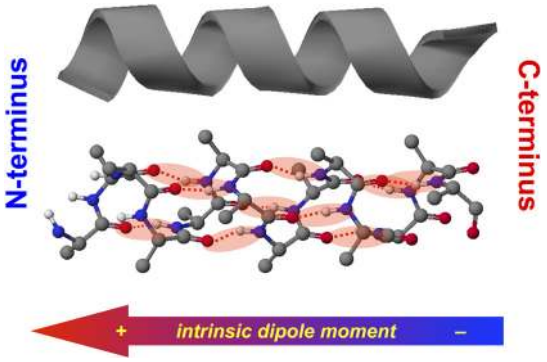

Fig. 2 Protein α-helix, ribbon diagram and ball and stick model with highlighted hydrogen-bond network.

broadband gap [or highest occupied molecular orbital (HOMO)–lowest unoccupied molecular orbital (LUMO) gap] of proteins, however, along with the inability to inject charges in them without chemically cleaving their backbones,[38–40] considerably limits their utility as electronic materials. Proteins and polypeptides (composed of native α-amino acids and their derivatives) mediate ET solely via tunneling, the efficiency of which is limited to about 2 nm.[41–46] Conversely, arrays of cofactors and redox-active residues, such as tryptophan or tyrosine, make it possible to attain long-range ET.[47,48] That is, multiple short and efficient "electron hopping" steps along arrays of redox moieties allow ET to exceed the 2-nm tunneling limit.[48–52]

Deoxyribonucleic acid (DNA) strands represent a class of biopolymers that can mediate CT at distances exceeding 2 nm.[53–57] Short efficient tunneling steps between closely situated bases, with relatively negative reduction potentials of their radical cations, mediate hole hopping. The lack of detectable distance dependence of the CT rates (for a donor–acceptor separation larger than about 1 nm) is an indication for the hopping mechanism. (In a case of tunneling, the CT rates, k_{CT}, fall off exponentially with donor–acceptor distance, $r(DA)$, i.e., $k_{CT} \propto \varepsilon^{-\beta r(DA)}$, while in a case of hopping, they fall off as an inverse of the number of hopping sites, N, i.e., $k_{CT} \propto 1/N^{\eta}$.)[49–51]

As an alternative to DNA, peptide nucleic acid (PNA) strands present certain advantages for long-range hole hopping.[58–61] The smaller helical twist of PNA, in comparison with DNA, improves the electronic coupling between neighboring bases.[58] Furthermore, PNA derivatives are not acids (despite the name) and they do not contain ionic charges along their backbones. Instead, PNA backbones comprise primary and secondary amides resulting in the intrinsic electric dipole reported for single-stranded structures.[62] The double-stranded PNA, however, has certain conformational rigidity and an advantage for CT over the single-stranded one. To attain permanent intrinsic dipoles in double-stranded structures, the PNA chains have to assemble in a parallel manner. Conversely, the antiparallel double-stranded PNA is slightly more stable than the parallel one.[63,64]

Considering the electronic features of the various natural macromolecular conjugates, we undertake a bioinspired approach to the development of molecular electrets that can mediate CT (Fig. 1).[3] Our *de novo* designs are based on derivatives of anthranilic acid, which is an aromatic β-amino acid. Similar to protein α- and 3_{10}-helices, Aa has ordered arrangements of amide and hydrogen bonds that result in permanent dipoles in the order of 4 to 5 D/residue pointing from the N- to the C-terminus (Fig. 1).[2,9] Unlike protein helices, however, the aromatic residues can provide sites for charge hopping along the Aa backbones. In DNA and PNA, the bases providing the charge hopping sites are electronically coupled via noncovalent face-to-face π-stacking. In Aa, the aromatic moieties compose the backbones and the partially π-conjugated covalent amide linkers ensure considerable overlap between the frontier orbitals on the neighboring residues.[9,65] Furthermore, the ability to adjust the electronic properties of each residue by synthetically altering the distal substituents (R_1 and R_2, Fig. 1) provides an incomparable unique means for tuning the CT mechanism from tunneling to hole hopping and to electron hopping.

3 Principles of Biodiversity Extended to Electronic Materials

The diversity of life on Earth is made possible through a variety of protein structures and functionalities that stem from only 20 common native α-amino acids. The sequence of amino acids in a protein chain directs the folds toward the preferred secondary conformations, tertiary structures, and quaternary self-assemblies that result in various protein functionalities. Cofactors and "noncommon" proteinogenic amino acids, such as selenocysteine and pyrrolysine, may appear as the centerpieces of observed protein activity. It is the whole protein microenvironment, however, with nanometer scale structural features that tunes the vital functionalities. Overall, the properties of the single side chain of each residue and its place in the protein sequence determine the emergence of the structure–function relationships at a macromolecular level. That is, altering the sequences comprising a few "common" residues that differ only by a single side chain leads to countless functionalities.

Can electronic and photonic material achieve the same diversity by employing similar principles? The bioinspired molecular electrets are composed of β-amino acids, i.e., Aa residues

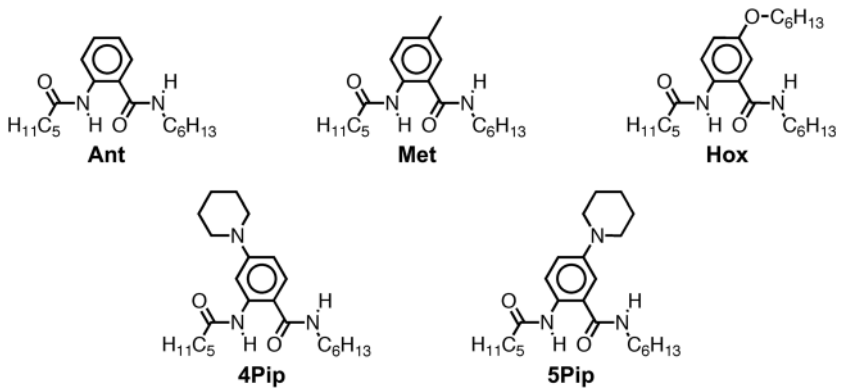

Fig. 3 Aa residues, with alkyl-terminated C- and N-termini, used for spectroscopic and electrochemical studies.

(Fig. 1). Each Aa residue has two side chains, R_1 and R_2 (Fig. 1), that can be synthetically modified (Fig. 3). The availability for variations at two sites, R_1 and R_2, provides a certain advantage over the native α-amino acids that contain only a single side chain each.

For hole-transducing molecular electrets, we prepared Aa residues with EDGs as the R_1 and R_2 substituents (Fig. 3). Replacing the hydrogen at R_2 with a strong EDG, such as dialkylamine, causes about 1 V negative shift in the reduction potentials [compare 5Pip and Ant, Figs. 3 and 4(b)]. This finding is in an agreement with the 1-eV elevation of the energy levels of the HOMOs induced by similar dialkylamine substituents,[9] i.e., such EDGs considerably improve the capabilities of the Aa residues to mediate hole transduction. The electrochemical reduction potentials of singly oxidized organic species, i.e., of $Aa^{\bullet+} + e^- \rightarrow Aa$, correlate with their ionization energies and hence, with the energy levels of their HOMOs.[66–68] Alkyl and alkyloxy substituents that are weaker EDGs than the amines also cause negative shifts in the reduction potential of Aa but not as large as the one observed for R_2 = dialkylamine [Fig. 4(b)].

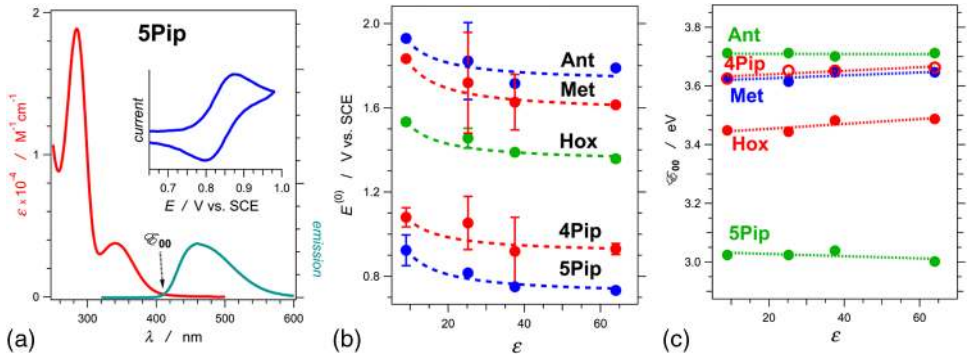

Fig. 4 Photophysical and electrochemical properties of different Aa residues (Fig. 3). (a) UV/visible absorption and fluorescence spectra of 5Pip for dichloromethane (DCM) (for fluorescence, $\lambda_{ex} = 310$ nm). The wavelength, λ_{00}, at the crossing point between the intensity-normalized spectra provides an estimate for the zero-to-zero energy, $\mathscr{E}_{00} = hc/\lambda_{00}$, which represents the highest occupied molecular orbital (HOMO)–lowest unoccupied molecular orbital (LUMO) optical gap.[5,65,69–71] Inset: cyclic voltammogram of 5Pip for DCM in the presence of 200 mM tetrabutylammonium hexafluorophosphate (scan rate = 200 mV/s). (b) Reduction potentials of singly oxidized Aa residues, $E^{(0)}$ ($Aa^{\bullet+} + e^- \rightarrow Aa$), obtained from cyclic voltammetry for solvents with different polarity (as represented by the solvent static relative dielectric constants, ε). The data points (the circles) represent $E^{(0)}$ for four neat solvents, obtained from extrapolation to zero electrolyte concentration.[72,73] The dashed lines are least-square data fits using $E = a + b/\varepsilon$, as expected from the Born solvation energy.[74] (c) Zero-to-zero energy of Aa residues. The circles are data points for four different solvents and dotted lines are linear data fits. [For (b) and (c), the four solvents with different ε are DCM, benzonitrile, acetonitrile, and propylene carbonate.]

Another feature of the electronic properties of the Aa residues is the significance of the exact position of the substituent; i.e., it is important not only what the substituent is but also where it is in the aromatic ring, i.e., R_1 versus R_2. Moving dialkylamine from the R_2 to the R_1 position causes about a 0.2-V positive shift in the reduction potential [Fig. 4(b)], making the Aa residue a slightly worse mediator of hole transduction.

The optical properties of the residues also manifest a strong dependence not only on the type of substituent but also on its position [Fig. 4(c)]. Thus, a single substituent for the two side chains, R_1 and R_2, of the Aa residues provide a means for tripling the diversity in properties compared to native amino acids with single side chains. For an electron-donating or electron-withdrawing substituent, G, the three possible Aa residues, $R_1 = G$, $R_2 = G$ and $R_1 = R_2 = G$, would have different electronic properties. This trend demonstrates one of the key advantages of bioinspired approaches versus the biomimetic and biological ones.[3]

An important feature revealed by the experimental findings is the difference in the extent with which the substituents affect the electrochemical and optical properties of the Aa residues. The reduction potentials of $Aa^{\bullet+}$, which correlate with the ionization energy of the residues, pronouncedly depend on the electron-donating strength of the substituents. The exact position of the substituents further tunes the ionization energy but it does not dominate the observed trend. That is, the negative shift in the reduction potential, $E^{(1/2)}(\mathrm{Ant}) > E^{(1/2)}(\mathrm{Met}) > E^{(1/2)}(\mathrm{Hox}) > E^{(1/2)}(4\mathrm{Pip}) > E^{(1/2)}(5\mathrm{Pip})$, follows the electron-donating strength of the substituent, $H < CH_3 < OC_6H_{13} < N(CH_2)_5$ [Fig. 4(b)]. The optical properties of the Aa residues, on the other hand, manifest a considerably stronger sensitivity to the position of the substituents than to their electron-donating strength or π-conjugating propensity. For the residues with substituents at position 5, Met, Hox and 5Pip (Fig. 3), the zero-to-zero energy, $\mathcal{E}_{00}$ (which is equivalent to optical band gap for molecular spectroscopy) decreases as R_2 alters from H to CH_3, OC_6H_{13}, and $N(CH_2)_5$ [Fig. 4(c)]. This trend follows the π-conjugating propensity of the substituents. Shifting the piperidine substituent from position 5 to 4 (i.e., 5Pip to 4Pip), increases $\mathcal{E}_{00}$ by about 0.6 eV, making it equivalent to $\mathcal{E}_{00}$ of Met [Fig. 4(c)]. Indeed, these trends are based on examining five conjugates, and their universality is still to be tested by expanding the set of Aa residues. Nevertheless, they reveal key design considerations for electronic and photonic organic materials.

Inducing CT rectification is the most important electronic feature of the molecular electrets. The intrinsic dipoles remove the degeneracy between the frontier orbitals on neighboring Aa residues resulting in "cascade" energy configurations for driving hole transfer or ET.[9] As the length of the molecular electrets increases above 10 nm or so, the energy of each of the frontier orbitals (e.g., HOMOs and LUMOs) should asymptotically approach constant values toward one of the termini due to dipole-induced charge displacement, making the "cascade" CT profiles nonlinear.

Once charge carriers are injected in a sequence of Aa residues, the intrinsic dipoles can ensure a preference for hole transfer toward the N-termini along the HOMOs of the residues, and for ET toward the C-termini along the LUMOs. The capability of Aa conjugates to act as molecular rectifiers (or diodes) can prove immensely beneficial for enhancing forward ET or hole transfer and suppressing undesired charge recombination. These rectifying properties can be attained with homomeric molecular electrets based on sequences of the same Aa residue selected for its ionization energy or electron affinity.

Conversely, at donor–acceptor interfaces, diversity in the electronic properties of the Aa residues can significantly aid the efficacy of the initial processes that convert the absorbed light energy into charge carriers. Coulomb trapping of charge-separation states at donor–acceptor interfaces is a principal source of losses in organic photovoltaic and other electronic devices.[14,75–83] It also imposes a need for larger driving forces than that required by the fundamental limits (decreasing, for example, the open circuit voltages, V_{OC}) in order to provide excess energy for the generated charges to escape the traps.[14,84–87] Even in the presence of favorably oriented dipoles, these trapping Coulomb interactions can extend over a nanometer or two from the donor–acceptor interfaces, and the depth of the Coulomb traps can be a few hundred millielectronvolts. Hence, because of the presence of such traps for the electret dipoles to exert a dominant effect, the electron or the hole has to migrate a couple of nanometers away from the countercharge at the donor–acceptor interface. Because the increment of Aa polyamides is about 0.45 nm/residue, the first two-to-four residues from the donor–acceptor interface are most

important for eliminating undesired Coulomb trapping. Considering, for example, hole hopping (i.e., on-resonance hole transfer) along Aa sequences, selecting the first few residues attached to the electron acceptor to have slightly higher ionization energies than the residues in the rest of the polyamide chain can decrease the depth of the Coulomb traps and even completely eliminate them. Molecular electrets with widely diverse sequences will allow for implementing this beneficial CT feature to different electronic materials and energy-conversion systems. In parallel with proteins and their amino-acid building blocks, such diversity in molecular electrets can originate from a few Aa residues with different ionization energies and electron affinities.

4 Experimental Methods

4.1 *Materials*

The synthetic starting materials and reagents were purchased from TCI America or Sigma-Aldrich. The solvents (reagent, high-performance-liquid-chromatography, and spectroscopic grade) were obtained from Fisher Scientific. The deuterated solvents were purchased from Cambridge Isotope.

The Aa residues (Fig. 3) are prepared from derivatives of 2-nitrobensoic acid with different R_1 and R_2 substituents (Fig. 1). A general synthetic route includes:[1,2] (1) attaching the desired R_1 and R_2 group, (2) coupling an alkylamine to the C-terminal carboxylate, (3) selectively reducing the nitro group to an amine, and (4) coupling an aliphatic carboxylic acid to the thus formed N-terminal amine. For Ant and Met, the precursors (2-nitrobenzoic acid and 5-methyl-2-nitrobenzoic acid) are commercially available, allowing for the elimination of step 1. All reactions are performed under a nitrogen atmosphere. To prevent undesired oxidation, step 4 is carried out immediately after step 3, without isolating the amine. The combined yields for steps 3 and 4 range between about 10% and 50% regardless of whether tin (II)[88] or zinc/ammonium formate[89] is used for the reduction of the nitrogroup.

All compounds are confirmed using NMR spectroscopy and high resolution mass spectrometry (HRMS). Chemical shifts are reported in parts per million relative to $CDCl_3$ (^{1}H, $\delta = 7.241$; ^{13}C, $\delta = 77.233$). Data for ^{1}H NMR are reported as follows: chemical shift, integration, multiplicity (s = singlet, d = doublet, t = triplet, q = quartet, p = pentaplet/quintet, m = multiplet), integration, and coupling constants. All ^{13}C NMR spectra were recorded with complete proton decoupling.

4.1.1 *Hexyl-N-hexanoylanthranilamide (Ant)*

The 3-mmol 2-nitrobenzoic acid and 6 mmol *N*-hydroxysuccinimide were dissolved in 10 ml *N*, *N*′-dimethylformamide (DMF). The solution was chilled on an ice bath and 9 mmol of an activation agent, *N*, *N*′-diisopropylcarbodiimide, was added dropwise. After stirring for 2 h at 0° C, 9 mmol of 1-aminohexane was added dropwise. The mixture was stirred for 30 more min at 0° C, allowed to warm up to room temperature and stirred until the completion of the reaction: the consumption of the nitrobenzoic acid was monitored using thin-layer chromatography (TLC). The reaction mixture was diluted with dichloromethane (DCM), washed with 5% HCl and MilliQ water, dried with anhydrous Na_2SO_4, concentrated *in vacu* and purified chromatographically to produce 550-mg white solid of *N*-hexyl-2-nitrobenzamide (2.2 mmol, 73% yield): ^{1}H-NMR (400 MHz, $CDCl_3$) δ/ppm: 7.90 (1 H, dd, $J_1 = 8.1$ Hz, $J_2 = 1.1$ Hz), 7.55 (1 H, td, $J_1 = 7.5$ Hz, $J_2 = 1.2$ Hz), 7.46 (1 H, td, $J_1 = 7.8$ Hz, $J_2 = 1.4$ Hz), 7.37 (1 H, dd, $J_1 = 7.5$ Hz, $J_2 = 1.4$ Hz), 6.40 (1 H, t, J = 6.0 Hz), 3.28 (2 H, td, $J_1 = 7.1$ Hz, $J_2 = 6.1$ Hz), 1.51 (2 H, p, $J = 7.2$ Hz), 1.26 (6 H, m), 0.84 (3 H, t, $J = 6.9$ Hz); ^{13}C-NMR (400 MHz, $CDCl_3$) δ/ppm: 166.61, 146.49, 133.69, 133.24, 130.30, 128.84, 124.44, 40.36, 31.58, 29.22, 26.67, 22.67, 14.14; HRMS m/z calculated for $C_{13}H_{19}N_2O_3^+$ $(M+H)^+$ 251.1396, found 251.1393 $(M+H)^+$.

N-hexyl-2-nitrobenzamide (1 mmol) and $SnCl_2 \cdot 2H_2O$ (sixfold molar excess) were suspended in 2 ml 1,2-dimethoxyethane and purged with nitrogen. The mixture was refluxed and the progress of the reaction was monitored with TLC. After complete reduction of the nitro group (usually about 2 to 5 h), the solvent was removed under reduced pressure, the reaction solid was suspended in 3 ml DMF under nitrogen, and 1.5 mmol hexanoic anhydride was

added dropwise, followed by a slow addition of 1.5 mmol triethylamine, and the mixture was stirred for 4 h. The reaction mixture was dissolved in 50 ml DCM, washed with a saturated aqueous solution of Na_2CO_3, and dried over anhydrous Na_2SO_4. Purification using flash chromatography resulted in 30 mg of white compound, Ant (0.9 mmol, 9% yield): ^{1}H-NMR (400 MHz, $CDCl_3$) δ/ppm: 11.00 (1 H, s), 8.56 (1 H, d, $J = 8.8$ Hz), 7.42 (2 H, m), 7.01 (1 H, s), 6.31 (1 H, s), 3.40 (2 H, q, $J = 6.7$ Hz), 2.36 (2 H, t, $J = 7.6$ Hz), 1.70 (2 H, p, $J = 7.5$ Hz), 1.60 (2 H, p, $J = 7.5$ Hz), 1.3 (10 H, m), 0.88 (6 H, t, $J = 7.0$ Hz); ^{13}C-NMR (400 MHz, $CDCl_3$) δ/ppm: 172.46, 169.21, 139.75, 132.58, 126.51, 122.72, 121.72, 120.83, 40.27, 38.69, 31.68, 31.59, 29.86, 26.87, 25.48, 22.78, 22.61, 14.22, 14.15; HRMS m/z calculated for $C_{19}H_{30}N_2NaO_2^+$ $(M + Na)^+$ 341.2199, found 341.2196 $(M + Na)^+$.

4.1.2 *Hexyl-N-hexanoyl-5-methylanthranilamide (Met)*

Starting with 5-methyl-2-nitrobenzoic acid and using the procedures for *N*-hexyl-2-nitrobenzamide, afforded *N*-hexyl-5-methyl-2-nitrobenzamide (21% yield): ^{1}H-NMR (400 MHz, $CDCl_3$) δ/ppm: 7.89 (1 H, d, $J = 8.4$ Hz), 7.27 (1 H, dd, $J_1 = 8.4$ Hz, $J_2 = 1.5$ Hz), 7.21 (1 H, d, $J =$ 1.5 Hz), 6.02 (1 H, s), 3.35 (2 H, q, $J = 7.1$ Hz), 2.40 (3 H, s), 1.56 (2 H, p, $J = 7.2$ Hz), 1.3 (6 H, m), 0.86 (3 H, t, $J = 6.8$ Hz);^{13}C-NMR (400 MHz, $CDCl_3$) δ/ppm: 166.96, 145.45, 144.08, 133.52, 130.73, 129.46, 124.72, 40.44, 31.64, 29.36, 26.76, 22.73, 21.54, 14.19; HRMS m/z calculated for $C_{14}H_{21}N_2O_3^+$ $(M + H)^+$ 265.1547, found 265.1556 $(M + H)^+$.

From *N*-hexyl-5-methyl-2-nitrobenzamide using the procedure for Ant, afforded Met with 25% yield: ^{1}H-NMR (400 MHz, $CDCl_3$) δ/ppm: 10.85 (1 H, s), 8.44 (1 H, dd, $J_1 = 8.5$ Hz, $J_2 = 2.8$ Hz), 7.23 (1 H, d, $J = 8.6$ Hz), 7.18 (1 H, d, $J = 1.9$ Hz), 6.24 (1 H, s), 3.39 (2 H, q, $J = 7.2$ Hz), 2.35 (2 H, t, $J = 7.6$ Hz), 2.29 (3 H, s), 1.70 (2 H, p, $J = 7.5$ Hz), 1.60 (2 H, p, $J = 7.4$ Hz), 1.3 (10 H, m), 0.88 (3 H, t, $J = 6.5$ Hz), 0.87 (3 H, t, $J = 6.7$ Hz); ^{13}C-NMR (400 MHz, $CDCl_3$) δ/ppm: 172.44, 169.29, 137.03, 133.07, 132.35, 126.95, 121.80, 121.09, 40.25, 38.56, 34.28, 31.67, 31.56, 29.64, 26.86, 25.50, 22.74, 22.57, 14.19, 14.11; HRMS m/z calculated for $C_{20}H_{32}N_2NaO_2^+$ $(M + Na)^+$ 355.2356, found 355.2371 $(M + Na)^+$.

4.1.3 *Hexyl-N-hexanoyl-4-(piperidin-N-yl)anthranilamide (4Pip)*

The 4-mmol 4-fluoro-2-nitrobenzoic acid was suspended in 2 ml piperidine and refluxed overnight. The reaction solution turned from clear to dark orange, indicative of the formation of 2-nitro-4-(piperidin-*N*-yl)benzoic acid. After cooling, the reaction solution was diluted with 100 ml DCM and sequentially washed with 1M HCl and brine. The organic layer was collected, dried over Na_2SO_4, and concentrated *in vacuo* to produce 980 mg yellow powder (3.9 mmol, 97%) of 2-nitro-4-(piperidin-*N*-yl)benzoic acid:^{1}H-NMR (400 MHz, $CDCl_3$) δ/ppm: 7.84 (1 H, d, $J = 9.2$ Hz), 6.87 (2 H, m), 3.38 (4 H, m), 1.67 (6 H, s); ^{13}C-NMR (400 MHz, $CDCl_3$) δ/ppm: 168.94, 154.18, 153.38, 133.58, 114.46, 107.88, 48.61, 25.35, 24.28; HRMS m/z calculated for $C_{12}H_{18}N_3O_4^+$ $(M + NH_4)^+$ 268.1292, found 268.1304 $(M + NH_4)^+$.

Using the thus obtained precursor for 4Pip, i.e., 2-nitro-4-(piperidin-*N*-yl)benzoic acid, with the procedure for *N*-hexyl-2-nitrobenzamide, afforded *N*-hexyl-2-nitro-4-(piperidin-*N*-yl)benzamide (yellow solid) with 75% yield: ^{1}H-NMR (400 MHz, $CDCl_3$) δ/ppm: 7.17 (2 H, m), 6.85 (1 H, dd, $J_1 = 8.6$ Hz, $J_2 = 2.6$ Hz), 5.46 (1 H, t, $J = 5.5$ Hz), 3.20 (6 H, m), 1.59 (6 H, m), 1.46 (2 H, p, $J = 6.6$ Hz), 1.22 (6 H, m), 0.81 (3 H, t, $J = 6.9$ Hz);^{13}C-NMR (400 MHz, $CDCl_3$) δ/ppm: 166.62, 152.28, 148.61, 129.51, 120.85, 117.79, 109.56, 48.96, 40.14, 31.54, 29.26, 26.62, 25.22, 24.08, 22.59, 14.06; HRMS m/z calculated for $C_{18}H_{28}N_3O_3^+$ $(M + H)^+$ 334.2125, found 334.2139 $(M + H)^+$.

Using the procedure for Ant with *N*-hexyl-2-nitro-4-(piperidin-*N*-yl)benzamide, afforded 4Pip with 21% yield: ^{1}H-NMR (400 MHz, $CDCl_3$) δ/ppm: 11.73 (1 H, s), 8.28 (1 H, d, $J = 2.6$ Hz), 7.29 (1 H, d, $J = 9.0$ Hz), 6.39 (2 H, m), 3.31 (2 H, q, $J = 6.7$ Hz), 3.22 (4 H, m), 2.33 (2 H, t, $J = 7.6$ Hz), 1.66 (2 H, p, $J = 7.5$ Hz), 1.55 (8 H, m), 1.27 (10 H, m), 0.83 (6 H, tt, $J_1 = 7.0$, $J_2 = 6.4$ Hz);^{13}C-NMR (400 MHz, $CDCl_3$) δ/ppm: 172.58, 169.20, 154.20, 142.05, 127.82, 108.41, 108.30, 105.81, 48.78, 39.94, 38.79, 31.62, 31.46, 29.72, 26.81, 25.50, 25.30, 24.46, 22.67, 22.53, 14.11, 14.03; HRMS m/z calculated for $C_{24}H_{39}N_3O_2^+$ $(M)^+$ 401.3037, found 401.3021 $(M)^+$.

4.1.4 *N-hexanoyl-5-(piperidin-N-yl)anthranilamide (5Pip)*

Starting with 4-fluoro-2-nitrobenzoic acid, 5Pip was prepared in four steps using a procedure similar to the one for 4Pip, as we have previously reported.[1]

4.1.5 *Hexyl-N-hexanoyl-5-hexyloxyanthranilamide (Hox)*

The 5-mmol 5-hydroxy-2-nitrobenzoic acid, 10 mmol Cs_2CO_3, and 11 mmol 1-iodohexane were suspended in 100-ml anhydrous *N*, *N*-dimethylacetamide and flushed with nitrogen. The reaction mixture immediately turned yellow due to the deprotonating of the hydroxyl group under the basic conditions (forming the *para*-nitrophenolate ion derivative of the starting material). The mixture was kept at 150°C for 3 h. Upon cooling, the reaction mixture was suspended in DCM, washed with acidic and basic aqueous solutions, and dried over anhydrous Na_2SO_4 to produce a slightly yellow oil. Purification using flash chromatography afforded 1.7 g (4.8 mmol, 96% yield) of hexyl-5-hexyloxy-2-nitrobenzoate: ^{1}H-NMR (400 MHz, $CDCl_3$) δ/ppm: 7.93 (1 H, d, $J = 9.0$ Hz), 6.97 (1 H, d, $J = 2.6$ Hz), 6.86 (1 H, dd, $J_1 = 9.0$ Hz, $J_2 = 2.7$ Hz), 4.27 (2 H, t, $J = 6.8$ Hz), 3.99 (2 H, t, $J = 6.5$ Hz), 1.75 (2 H, p, $J = 7.0$ Hz), 1.66 (2 H, p, $J = 7.3$ Hz), 1.40 (2 H, m), 1.3 (10 H, m), 0.83 (6 H, tt, $J = 7.0$ Hz); ^{13}C-NMR (400 MHz, $CDCl_3$) δ/ppm: 166.27, 163.10, 139.79, 131.63, 126.66, 115.84, 114.69, 69.28, 66.72, 31.51, 31.45, 28.91, 28.31, 25.60, 25.56, 22.61, 22.58, 14.03; HRMS m/z calculated for $C_{19}H_{30}NO_5^+$ $(M + H)^+$ 352.2118, found 352.2118 $(M + H)^+$.

Hexyl-5-hexyloxy-2-nitrobenzoate (930 mg, 2.6 mmol) was dissolved in 2 ml ethanol and while stirring, 1 ml of 3 M KOH in ethanol was added dropwise. The basified solution was heated to 60°C. The progress of the reaction was monitored using TLC. After the complete consumption of the starting material, the reaction solution was allowed to cool to room temperature and quenched by slowly adding it to a mixture of DCM and 5% aqueous HCl. The organic phase was collected, washed with MilliQ water, dried over anhydrous Na_2SO_4, and concentrated *in vacuo* to produce white solid (640 mg, 2.4 mmol, 92%) of 5-hexyloxy-2-nitrobenzoic acid:^{1}H-NMR (400 MHz, $CDCl_3$) δ/ppm: 8.01 (1 H, d, $J = 9.1$ Hz), 7.13 (1 H, d, $J = 2.7$ Hz), 7.02 (1 H, dd, $J_1 = 9.1$ Hz, $J_2 = 2.7$ Hz), 4.05 (2 H, t, $J = 6.5$ Hz), 1.81 (2 H, p, $J = 7.1$ Hz), 1.45 (2 H, p, $J = 7.1$ Hz), 1.32 (4 H, m), 0.89 (3 H, t, $J = 6.9$ Hz); ^{13}C-NMR (400 MHz, $CDCl_3$) δ/ppm: 170.89, 163.12, 140.09, 130.38, 126.81, 116.74, 114.92, 69.49, 31.60, 29.00, 25.69, 22.71, 14.15; HRMS m/z calculated for $C_{13}H_{18}NO_5^+$ $(M + H)^+$ 268.1179, found 268.1192 $(M + H)^+$.

Under nitrogen, 5-hexyloxy-2-nitrobenzoic acid (424 mg, 1.2 mmol), ammonium formate (760 mg, 12 mmol) and zinc dust (434 mg, 6.7 mmol) were suspended in 4 ml 1,2-dimethoxyethane and stirred for 6 h. The reaction mixture was filtered and the filtrate was diluted with DCM then washed in 1% HCl and MilliQ water. The solvent was removed *in vacuo* and 2 ml of DMF was added under nitrogen. Sequentially, hexanoic anhydride (0.23 ml, 1 mmol) and Et_3N (0.14 ml, 1 mmol) were added dropwise and the mixture was stirred at room temperature for 2 h. The reaction mixture was diluted with 50 ml ethyl acetate, washed with 5% HCl and MilliQ water, dried over Na_2SO_4, and concentrated *in vacuo*. Purification using flash chromatography afforded 210 mg white solid (0.48 mmol, 40% yield) of Hox: ^{1}H-NMR (400 MHz, $CDCl_3$) δ/ppm: 10.56 (1 H, s), 8.28 (1 H, d, $J = 9.1$ Hz), 6.91 (1 H, d, $J = 2.8$ Hz), 6.86 (1 H, dd, $J_1 = 9.1$ Hz, $J_2 = 2.8$ Hz), 6.79 (1 H, t, $J = 5.2$ Hz), 3.84 (2 H, t, $J = 6.6$ Hz), 3.32 (2 H, q, $J = 6.7$ Hz), 2.28 (2 H, t, $J = 7.7$ Hz), 1.65 (4 H, m), 1.55 (2 H, p, $J = 7.3$ Hz), 1.3 (16 H, m), 0.84 (9 H, t, $J = 6.5$ Hz); ^{13}C-NMR (400 MHz, $CDCl_3$) δ/ppm: 172.15, 168.88, 154.44, 132.19, 123.13, 122.86, 117.11, 113.52, 68.57, 40.21, 38.35, 31.70, 31.63, 31.53, 29.53, 29.35, 26.83, 25.80, 25.48, 22.70, 22.52, 14.13, 14.05; HRMS m/z calculated for $C_{25}H_{42}N_2NaO_3^+$ $(M + Na)^+$ 441.3088, found 441.3109 $(M + Na)^+$.

4.2 *Methods*

4.2.1 *UV/visible absorption and emission spectroscopy*

The ground-state absorption spectra were recorded in a transmission mode using a JASCO V-670 spectrophotometer (Tokyo, Japan); and the emission spectra were collected with a

FluoroLog-3 spectrofluorometer (Horiba-Jobin-Yvon, Edison, New Jersey) as previously reported.[90–96]

4.2.2 *Electrochemical measurements*

Cyclic voltammetry (CV) was conducted using Reference 600™ Potentiostat/Galvanostat/ZRA (Gamry Instruments, Pennsylvania), equipped with a three-electrode cell, as previously described.[72,73] The half-wave potentials, $E^{(1/2)}$, were determined from the midpoints between the cathodic and anodic peak potentials for reversible oxidation and from the inflection points of the anodic waves for irreversible oxidation. For each residue, CV was carried out for different solvents at different electrolyte concentrations (tetrabutylammonium hexafluorophosphate was used for the electrolyte with concentration varying between 25 to 200 mM). At least three voltammograms (scan rate = 200 mV s^{-1}) were recorded for each sample condition (Aa residue, solvent and electrolyte concentration). From the dependence of $E^{(1/2)}$ on the electrolyte concentration, the potentials for neat solvents were estimated from extrapolations to zero[73] and presented in Fig. 4(b).

5 Conclusions

Inducing rectification and managing charge traps (and potential barriers along CT pathways) represent only a couple of examples of the promising features of molecular electrets. Sets of non-native Aa residues, therefore, can serve as principal tools for the development of widely diverse molecular electrets and provide venues for bottom-up designs of functional electronic and photonic materials for energy applications.

Acknowledgments

Funding for this work was provided by the USA National Science Foundation (grants CHE 1465284, CBET 0935995 and CBET 0923408, as well as IGERT DGE 0903667 for J. M. L); and by the UCR Office of Research and Economic Development for their FY14-15 Proof of Concept Award (V. I. V.) and Collaborative Seed Grant (B. A. and V. I. V.)

References

1. D. Bao et al., "Dipole-mediated rectification of intramolecular photoinduced charge separation and charge recombination," *J. Am. Chem. Soc.* **136**, 12966–12973 (2014).
2. B. Xia et al., "Anthranilamides as bioinspired molecular electrets: experimental evidence for a permanent ground-state electric dipole moment," *J. Org. Chem.* **78**, 1994–2004 (2013).
3. V. I. Vullev, "From biomimesis to bioinspiration: what's the benefit for solar energy conversion applications?" *J. Phys. Chem. Lett.* **2**, 503–508 (2011).
4. N. Camaioni and R. Po, "Pushing the envelope of the intrinsic limitation of organic solar cells," *J. Phys. Chem. Lett.* **4**, 1821–1828 (2013).
5. S. Guo et al., "Photoinduced electron transfer between pyridine coated cadmium selenide quantum dots and single sheet graphene," *Adv. Funct. Mater.* **23**, 5199–5211 (2013).
6. H. Lu et al., "Pyridine-coated lead sulfide quantum dots for polymer hybrid photovoltaic devices," *Adv. Sci. Lett.* **3**, 101–109 (2010).
7. W. Wang et al., "Hybrid low resistance ultracapacitor electrodes based on 1-pyrene butyric acid functionalized centimeter-scale graphene sheets," *J. Nanosci. Nanotechnol.* **12**, 6913–6920 (2012).
8. J. Lin et al., "Supercapacitors based on pillared graphene nanostructures," *J. Nanosci. Nanotechnol.* **12**, 1770–1775 (2012).
9. M. K. Ashraf et al., "Theoretical design of bioinspired macromolecular electrets based on anthranilamide derivatives," *Biotechnol. Prog.* **25**, 915–922 (2009).

10. H. D. Sikes et al., "Rapid electron tunneling through oligophenylenevinylene bridges," *Science* **291**, 1519–1523 (2001).
11. S. Y. Sayed et al., "Charge transport in molecular electronic junctions: Compression of the molecular tunnel barrier in the strong coupling regime," *Proc. Natl Acad. Sci. USA* **109**, 11498–11503 (2012).
12. J. R. Heath and M. A. Ratner, "Molecular electronics," *Phys. Today* **56**, 43–49 (2003).
13. J. A. Christians and P. V. Kamat, "Trap and transfer. Two-step hole injection across the Sb_2S_3/CuSCN interface in solid-state solar cells," *ACS Nano* **7**, 7967–7974 (2013).
14. X. Y. Zhu, Q. Yang, and M. Muntwiler, "Charge-transfer excitons at organic semiconductor surfaces and interfaces," *Acc. Chem. Res.* **42**, 1779–1787 (2009).
15. S. Upadhyayula et al., "Coatings of polyethylene glycol for suppressing adhesion between solid microspheres and flat surfaces," *Langmuir* **28**, 5059–5069 (2012).
16. J. Wan et al., "Surface-bound proteins with preserved functionality," *Ann. Biomed. Eng.* **37**, 1190–1205 (2009).
17. B. Millare et al., "Dependence of the quality of adhesion between polydimethyl siloxane and glass surfaces on the conditions of treatment with oxygen plasma," *Langmuir* **24**, 13218–13224 (2008).
18. W. J. Jasper et al., "Degradation processes in corona-charged electret filter-media with exposure to ethyl benzene," *J. Eng. Fibers Fabrics* **2**(4), 19–24 (2007).
19. G. M. Sessler, "Electrets: recent developments," *J. Electrostat.* **51**, 137–145 (2001).
20. L. S. McCarty and G. M. Whitesides, "Electrostatic charging due to separation of ions at interfaces: contact electrification of ionic electrets," *Angew. Chem. Int. Ed.* **47**, 2188–2207 (2008).
21. R. Kressmann, G. M. Sessler, and P. Gunther, "Space-charge electrets," *IEEE Trans. Dielect. Electr. Insul.* **3**, 607–623 (1996).
22. R. P. Feynman et al., *The Feynman Lectures on Physics: Mainly Electromagnetism and Matter*, Vol. **2**, Addison-Wesley Publishing Company, Boston, MA (1977).
23. S. Upadhyayula et al., "Permanent electric dipole moments of carboxyamides in condensed media: what are the limitations of theory and experiment?" *J. Phys. Chem. B* **115**, 9473–9490 (2011).
24. W. G. J. Hol, P. T. Van Duijnen, and H. J. C. Berendsen, "The alpha-helix dipole and the properties of proteins," *Nature* **273**, 443–446 (1978).
25. W. G. J. Hol, "Effects of the alpha-helix dipole upon the functioning and structure of proteins and peptides," *Adv. Biophys.* **19**, 133–165 (1985).
26. A. Wada, "Dielectric properties of polypeptide solutions. II. Relation between the electric dipole moment and the molecular weight of the alpha-helix," *J. Chem. Phys.* **30**, 328–329 (1959).
27. Y.-G. K. Shin et al., "Distance dependence of electron transfer across peptides with different secondary structures: the role of peptide energetics and electronic coupling," *J. Am. Chem. Soc.* **125**, 3722–3732 (2003).
28. D. A. Doyle et al., "The structure of the potassium channel: molecular basis of K+ conduction and selectivity," *Science* **280**, 69–77 (1998).
29. R. Dutzler et al., "X-ray structure of a ClC chloride channel at 3.0 Å reveals the molecular basis of anion selectivity," *Nature* **415**, 287–294 (2002).
30. X. H. Chen et al., "Alpha-helix C-terminus acting as a relay to mediate long-range hole migration in proteins," *J. Phys. Chem. Lett.* **1**, 1637–1641 (2010).
31. S. Tanaka and R. A. Marcus, "Electron transfer model for the electric field effect on quantum yield of charge separation in bacterial photosynthetic reaction centers," *J. Phys. Chem. B* **101**, 5031–5045 (1997).
32. E. Galoppini and M. A. Fox, "Effect of the electric field generated by the helix dipole on photoinduced intramolecular electron transfer in dichromophoric alpha-helical peptides," *J. Am. Chem. Soc.* **118**, 2299–2300 (1996).
33. M. A. Fox and E. Galoppini, "Electric field effects on electron transfer rates in dichromophoric peptides: the effect of helix unfolding," *J. Am. Chem. Soc.* **119**, 5277–5285 (1997).
34. S. Yasutomi et al., "A molecular photodiode system that can switch photocurrent direction," *Science* **304**, 1944–1947 (2004).

35. L. Garbuio et al., "Effect of orientation of the peptide-bridge dipole moment on the properties of fullerene-peptide-radical systems," *J. Am. Chem. Soc.* **134**, 10628–10637 (2012).
36. H. S. Mandal and H. B. Kraatz, "Electron transfer across alpha-helical peptides: potential influence of molecular dynamics," *Chem. Phys.* **326**, 246–251 (2006).
37. C. Shlizerman et al., "*De novo* designed coiled-coil proteins with variable conformations as components of molecular electronic devices," *J. Am. Chem. Soc.* **132**, 5070–5076 (2010).
38. J. F. Odonnell and C. K. Mann, "Controlled-potential oxidation of aliphatic amides," *J. Electroanal. Chem.* **13**, 157–162 (1967).
39. L. G. Fong et al., "Nonenzymatic oxidative cleavage of peptide-bonds in apoprotein-B-100," *J. Lipid Res.* **28**(12), 1466–1477 (1987).
40. M. J. Davies, "Protein and peptide alkoxyl radicals can give rise to C-terminal decarboxylation and backbone cleavage," *Arch. Biochem. Biophys.* **336**, 163–172 (1996).
41. D. N. Beratan et al., "Electron-tunneling pathways in proteins," *Science* **258**, 1740–1741 (1992).
42. H. B. Gray and J. R. Winkler, "Long-range electron transfer," *Proc. Natl Acad. Sci. USA* **102**, 3534–3539 (2005).
43. V. I. Vullev and G. Jones II, "Photoinduced charge transfer in helical polypeptides," *Res. Chem. Intermed.* **28**, 795–815 (2002).
44. G. Jones, II, X. Zhou, and V. I. Vullev, "Photoinduced electron transfer in alpha-helical polypeptides: dependence on conformation and electron donor-acceptor distance," *Photochem. Photobiol. Sci.* **2**, 1080–1087 (2003).
45. G. Jones, II and V. I. Vullev, "Photoinduced electron transfer between non-native donor-acceptor moieties incorporated in synthetic polypeptide aggregates," *Org. Lett.* **4**, 4001–4004 (2002).
46. G. Jones, II et al., "Multistep photoinduced electron transfer in a de novo helix bundle: multimer self-assembly of peptide chains including a chromophore special pair," *J. Am. Chem. Soc.* **122**, 388–389 (2000).
47. C. Shih et al., "Tryptophan-accelerated electron flow through proteins," *Science* **320**, 1760–1762 (2008).
48. J. J. Warren, J. R. Winkler, and H. B. Gray, "Hopping maps for photosynthetic reaction centers," *Coord. Chem. Rev.* **257**, 165–170 (2013).
49. J. Jortner et al., "Charge transfer and transport in DNA," *Proc. Natl Acad. Sci. USA* **95**, 12759–12765 (1998).
50. K. Kawai et al., "Kinetics of weak distance-dependent hole transfer in DNA by adenine-hopping mechanism," *J. Am. Chem. Soc.* **125**, 6842–6843 (2003).
51. C. Behrens et al., "Weak distance dependence of excess electron transfer in DNA," *Angew. Chem. Int. Ed.* **41**, 1763–1766 (2002).
52. G. Jones, II et al., "Photoactive peptides. 6. Photoinduced electron transfer for pyrenesulfonamide conjugates of tryptophan-containing peptides. Mitigation of fluoroprobe behavior in N-terminal labeling experiments," *Bioorg. Med. Chem. Lett.* **5**, 2385–2390 (1995).
53. F. D. Lewis, "Distance-dependent electronic interactions across DNA base pairs: charge transport, exciton coupling, and energy transfer," *Isr. J. Chem.* **53**, 350–365 (2013).
54. K. Kawai and T. Majima, "Hole transfer kinetics of DNA," *Acc. Chem. Res.* **46**, 2616–2625 (2013).
55. N. Renaud et al., "Between superexchange and hopping: an intermediate charge-transfer mechanism in poly(A)-poly(T) DNA hairpins," *J. Am. Chem. Soc.* **135**, 3953–3963 (2013).
56. F. D. Lewis et al., "Crossover from superexchange to hopping as the mechanism for photoinduced charge transfer in DNA hairpin conjugates," *J. Am. Chem. Soc.* **128**, 791–800 (2006).
57. K. Senthilkumar et al., "Absolute rates of hole transfer in DNA," *J. Am. Chem. Soc.* **127**, 14894–14903 (2005).
58. R. Venkatramani et al., "Nucleic acid charge transfer: black, white and gray," *Coord. Chem. Rev.* **255**, 635–648 (2011).
59. E. Hatcher et al., "PNA versus DNA: effects of structural fluctuations on electronic structure and hole-transport mechanisms," *J. Am. Chem. Soc.* **130**, 11752–11761 (2008).

60. R. Venkatramani et al., "Evidence for a near-resonant charge transfer mechanism for double-stranded peptide nucleic acid," *J. Am. Chem. Soc.* **133**, 62–72 (2011).
61. E. Wierzbinski et al., "The single-molecule conductance and electrochemical electron-transfer rate are related by a power law," *ACS Nano* **7**, 5391–5401 (2013).
62. M. A. Wolak et al., "Electronic structure of self-assembled peptide nucleic acid thin films," *J. Phys. Chem. C* **115**, 17123–17135 (2011).
63. M. Egholm et al., "PNA hybridizes to complementary oligonucleotides obeying the Watson-Crick hydrogen-bonding rules," *Nature* **365**, 566–568 (1993).
64. P. E. Nielsen and G. Haaima, "Peptide nucleic acid (PNA). A DNA mimic with a pseudopeptide backbone," *Chem. Soc. Rev.* **26**, 73–78 (1997).
65. J. Wan et al., "Solvent dependence of the charge-transfer properties of a quaterthiophene-anthraquinone dyad," *J. Photochem. Photobiol. A* **197**, 364–374 (2008).
66. H. D. Burrows, "The relation between standard electrode and ionization potentials of metal ions," *J. Chem. Educ.* **53**, 365 (1976).
67. A. Dhiman et al., "A simple correlation of anodic peak potentials of silylarenes and their vertical ionization energies," *Organometallics* **23**, 1636–1638 (2004).
68. P. Muller, "Glossary of terms used in physical organic-chemistry," *Pure Appl. Chem.* **66**, 1077–1184 (1994).
69. J. Hu et al., "Long-lived photogenerated states of α-oligothiophene-acridinium dyads have triplet character," *J. Phys. Chem. A* **113**, 3096–3107 (2009).
70. V. I. Vullev and G. Jones, "Photoinduced electron transfer in alkanoylpyrene aggregates in conjugated polypeptides," *Tetrahedr. Lett.* **43**, 8611–8615 (2002).
71. G. Jones, II et al., "Photoinduced electron transfer in arylacridinium conjugates in a solid glass matrix," *J. Phys. Chem. B* **111**, 6921–6929 (2007).
72. D. Bao et al., "Electrochemical reduction of quinones: interfacing experiment and theory for defining effective radii of redox moieties," *J. Phys. Chem. B* **114**, 14467–14479 (2010).
73. D. Bao et al., "Electrochemical oxidation of ferrocene: a strong dependence on the concentration of the supporting electrolyte for nonpolar solvents," *J. Phys. Chem. A* **113**, 1259–1267 (2009).
74. M. Born, "Volumes and heats of hydration of ions," *Z. Phys.* **1**, 45–48 (1920).
75. Q. Yang, M. Muntwiler, and X. Y. Zhu, "Charge transfer excitons and image potential states on organic semiconductor surfaces," *Phys. Rev. B* **80**, 115214 (2009).
76. I. Lalov, C. Warns, and P. Reineker, "Model of mixed Frenkel and charge-transfer excitons in donor-acceptor molecular crystals: investigation of vibronic spectra," *New J. Phys.* **10**, 085006 (2008).
77. M. Muntwiler, Q. Yang, and X. Y. Zhu, "Exciton dynamics at interfaces of organic semiconductors," *J. Electron Spectrosc. Relat. Phenom.* **174**, 116–124 (2009).
78. M. Yokoyama et al., "Mechanism of photocarrier generation in polyvinylcarbazole. Mechanism of extrinsic carrier photogeneration. Quenching of exciplex fluorescence by electric field," *Polym. Prepr. (Am. Chem. Soc., Div. Polym. Chem.)* **20**(April), 399–402 (1979).
79. M. Yokoyama et al., "Mechanism of extrinsic carrier photogeneration in poly-N-vinylcarbazole. II. Quenching of exciplex fluorescence by electric field," *J. Chem. Phys.* **75**, 3006–3011 (1981).
80. M. Yokoyama, Y. Endo, and H. Mikawa, "Quenching of exciplex fluorescence by an electric field in the solid state," *Chem. Phys. Lett.* **34**, 597–600 (1975).
81. J. P. Schmidtke, R. H. Friend, and C. Silva, "Tuning interfacial charge-transfer excitons at polymer-polymer heterojunctions under hydrostatic pressure," *Phys. Rev. Lett.* **100**, 157401 (2008).
82. P. Peumans and S. R. Forrest, "Separation of geminate charge-pairs at donor-acceptor interfaces in disordered solids," *Chem. Phys. Lett.* **398**, 27–31 (2004).
83. U. Albrecht and H. Baessler, "Yield of geminate pair dissociation in an energetically random hopping system," *Chem. Phys. Lett.* **235**, 389–393 (1995).
84. R. D. Pensack and J. B. Asbury, "Beyond the adiabatic limit: charge photogeneration in organic photovoltaic materials," *J. Phys. Chem. Lett.* **1**, 2255–2263 (2010).

85. J. Guo et al., "Charge generation and recombination dynamics in poly(3-hexylthiophene)/fullerene blend films with different regioregularities and morphologies," *J. Am. Chem. Soc.* **132**, 6154–6164 (2010).
86. M. Muntwiler et al., "Coulomb barrier for charge separation at an organic semiconductor interface," *Phys. Rev. Lett.* **101** (2008).
87. H. Scher and S. Rackovsky, "Theory of geminate recombination on a lattice," *J. Chem. Phys.* **81**, 1994–2009 (1984).
88. F. D. Bellamy and K. Ou, "Selective reduction of aromatic nitro compounds with stannous chloride in nonacidic and nonaqueous medium," *Tetrahedr. Lett.* **25**, 839–842 (1984).
89. D. C. Gowda, B. Mahesh, and S. Gowda, "Zinc-catalyzed ammonium formate reductions: rapid and selective reduction of aliphatic and aromatic nitro compounds," *Ind. J. Chem. B* **40B**(1), 75–77 (2001).
90. J. M. Vasquez et al., "Fluorescence enhancement of warfarin induced by interaction with beta-cyclodextrin," *Biotechnol. Prog.* **25**, 906–914 (2009).
91. S. Upadhyayula et al., "Photoinduced dynamics of a cyanine dye: parallel pathways of non-radiative deactivation involving multiple excited-state twisted transients," *Chem. Sci.* **6**, 2237–2251 (2015).
92. B. Jung, V. I. Vullev, and B. Anvari, "Revisiting indocyanine green: effects of serum and physiological temperature on absorption and fluorescence characteristics," *IEEE J. Sel. Top. Quantum Electron.* **20**(2), 7000409 (2014).
93. V. Nuñez et al., "Microfluidic space-domain time-resolved emission spectroscopy of terbium(III) and europium(III) chelates with pyridine-2,6-dicarboxylate," *Anal. Chem.* **85**, 4567–4577 (2013).
94. M. Ghazinejad et al., "Non-invasive high-throughput metrology of functionalized graphene sheets," *Adv. Funct. Mater.* **22**, 4519–4525 (2012).
95. B. Xia et al., "Amyloid histology stain for rapid bacterial endospore imaging," *J. Clin. Microbiol.* **49**, 2966–2975 (2011).
96. M. S. Thomas et al., "Kinetics of bacterial fluorescence staining with 3,3'-diethylthiacyanine," *Langmuir* **26**, 9756–9765 (2010).

Jillian M. Larsen is a senior PhD student in bioengineering at the University of California, Riverside (UCR). She received her BS degree in biochemistry from UCR. Her current research is on the design, preparation, and characterization of dipolar organic conjugates. She developed several procedures, including microwave-aided procedures, for the synthesis of anthranilamides and their precursors.

Eli M. Espinoza is a PhD student in chemistry at the University of California, Riverside. He received his BS degree from Azusa Pacific University and his MS degree in chemistry from California State University, Los Angeles. His current research is on synthesis, electrochemistry, and spectroscopy of organic conjugates for photonic and electronic materials. He develops procedures for preparing multifunctional polyaromatics with pronounced regioisomer purity.

Valentine I. Vullev is an associate professor at the University of California, Riverside. He received his PhD in chemistry from Boston University and carried out postdoctoral work at Harvard University. His research interests are in charge transfer, photonics, organic electronic materials, and molecular engineering.